Polímeros
ISSN 1678-5169 (Online)

https://doi.org/10.1590/0104-1428.20240032

ORIGINAL ARTICLES

Processing and characterization of biocomposites based on polylactic acid and coconut by-products

Yulinali Valente Morales[1], Luz del Carmen Montoya-Ballesteros[1], Luis Enrique Robles-Ozuna[1], Yesica Yudith Martínez Núñez[1], Judith Fortiz Hernández[1], José Carmelo Encinas-Encinas[2] and Tomás Jesús Madera-Santana[1*]

[1]Coordinación de Tecnología de Alimentos de Origen Vegetal, Centro de Investigación en Alimentación y Desarrollo A.C., Hermosillo, Sonora, México

[2]Departamento de Investigación en Polímeros y Materiales, Universidad de Sonora, Hermosillo, Sonora, México

**madera@ciad.mx*

Abstract

Coconut mesocarp fiber (CMF) is a by-product of the coconut industry; it was milled to produce coconut mesocarp particles (CMP). The main elements identified in CMP samples were C and O, which represent 96.75%. The CMP were mixed with a polylactic acid (PLA) matrix by extrusion. The mechanical, thermal, structural, and morphological properties of four biocomposites with 0, 2, 5, and 8 wt% CMP (CMP0, CMP2, CMP5, and CMP8, respectively) were determined. The biocomposites showed a decrease in tensile strength, elongation at break, and elastic modulus values as the CMP content increased, except for CMP5, which showed a higher elastic modulus than the PLA matrix. The thermal analysis showed that the biocomposites presented better thermal stability than the PLA matrix. CMP2 and CMP5 had rough surfaces, while CMP8 had weaker fracture zones.

Keywords: *composite materials, agroindustrial by-product, morphological analysis, physicochemical properties, bioplastic matrix.*

How to cite: Valente Morales, Y., Montoya-Ballesteros, L. C., Robles-Ozuna, L. E., Martínez Núñez, Y. Y., Fortiz Hernández, J., Encinas-Encinas, J. C., & Madera-Santana, T. J. (2024). Processing and characterization of biocomposites based on polylactic acid and coconut by-products. *Polímeros: Ciência e Tecnologia*, *34*(2), e20240020.

1. Introduction

Agro-industrial wastes represent a major environmental pollution problem: They impact different ecosystems through final disposal in confinement sites, open dumps, or water bodies. Untreated agro-industrial wastes, including undesirable by-products, contribute to the emission of greenhouse gases, which exacerbate climate change in various ways[1]. Agro-industrial residues contain a high content of organic matter, which is rich in carbohydrates, proteins, lipids, fibers, phenolic compounds, and bioactive compounds[2]. These products can be used to fabricate biocomposites due to their high availability and low price, making them a highly sustainable strategy for waste valorization[3]. Moreover, they represent an ecological and unique option to reinforce bioplastic matrices, such as polylactic acid (PLA), which is a biodegradable under compostable conditions and can be employed as a matrix or binding agent for the development of biocomposites[4].

Coconut (*Cocos nucifera* L.) is one of the most important crops in tropical areas. It grows in 93 countries around the world, including Mexico. The growing demand for coconut consumption has turned it into a commercially important crop that contributes to the growth of national economies. Each year, 55 billion coconuts are processed throughout the world, generating a large volume of waste, including coconut residues (mesocarp), shells, and inner kernels (endocarp). This disposal represents a waste of natural resources and a source environmental pollution[3,5]. Coconut fiber, also known as "coconut coir", is present in the mesocarp and represents around 35% of the coconut. It is a hard, resistant, and light fiber that has resistance to abrasion and good thermal stability due to its high lignin content (26.43%)[3]. However, no studies exist on coconut mesocarp particles (CMP) by-products to develop biocomposites using PLA as a polymeric matrix.

The aim of this study was to develop and characterize new biocomposites based on coconut mesocarp particles (CMP) of the Alto Pacifico 2 variety and PLA as matrix. The proximal and physicochemical characteristics of the CMP were determined. The PLA-CMP biocomposites were produced by extrusion in a flat die profile to obtain laminated biocomposites. Mechanical, chemical, structural, and morphological properties were determined for PLA-CMP biocomposites. The addition of CMP to a PLA matrix produces biodegradable biocomposites with excellent mechanical and thermal properties.

2. Materials and Methods

2.1. Materials

Coconut mesocarp fiber (CMF) was obtained from Alto Pacifico 2 coconuts at port of San Crisanto, Yucatán. CMF was sun-dried for one week until it reached a moisture content of 7.67%. Then, CMF was ground in an industrial knife mill (Pagani model 1620, Mexico City, Mexico); a second grinding was carried out in a Comitrol 3600 mill (Urschel Laboratories Inc., Chesterton, IN, USA). The ground CMF was subjected to a size reduction via a hammer mill (model DF-15, Dade, Shenzhen, China). After milling, the product was sieved through a Tyler No. 100 mesh to obtain small particles, which were called coconut mesocarp particles (CMP). Polylactic acid (Ingeo 4043D) from NatureWorks LLC. (Minnetonka, MN, USA) was used as the polymeric matrix.

2.2. Physicochemical characterization

The proximate composition of CMP—including moisture, ash, protein, ethereal extract, crude fiber, and nitrogen-free extract were determined by using the official methods of AOAC International.

Fourier transform infrared spectroscopy (FTIR) was performed using the attenuated total reflection (ATR) accessory of a Thermo Nicolet Nexus 670-FTIR spectrophotometer (Madison, WI, USA). The CMP spectra were obtained in the 4000-600 cm^{-1} range, at 4 cm^{-1} resolution, and with 64 scans.

To measure phenolic compounds in CMP, 25 mg of the dry sample was weighed and added to 5 mL of an 80% methanol solution was added. The mixture was agitated for 4 min. Subsequently, it was centrifuged at 1100 *g* for 10 min at room temperature (25°C), and the supernatant was removed and stored. The residue was subjected to four extractions, each with 5 mL of 80% methanol, and the supernatants were pooled. The total phenolic contents was determined with the Folin–Ciocalteu method as described by Singleton et al.[6], with some modifications. Briefly, 100 µL of sample, 600 µL of distilled water, and 50 µL of Folin–Ciocalteu reagent were incubated in a test tube for 5 min. Subsequently, 150 µL of sodium carbonate was added. After incubation for 2 h in the dark, the absorbance was read at 760 nm. A gallic acid standard curve was used to determine the total phenolic content. The results are expressed as mg gallic acid/g sample on a dry basis.

2.3. Morphological characterization

FEI XL30 environmental scanning electron microscope (Philips Corp. –FEG, Hillsboro, OR, USA) was used for morphological analysis of CMP. The samples were coated with a layer of gold-palladium with an Au-Pd layer with a QI5OR-ES plasma generator (Quorum, Sussex, UK). The morphological analysis of the PLA–CMP biocomposites in their tensile fracture zone was performed. The elemental composition of the CMP was determined using a JEOL energy dispersive X-ray spectrometer (EDS) on JSM 7900F FSEM equipment (Zaventem, Belgium), which had a 30 kV acceleration.

2.4. Processing of the biocomposites

The PLA-CMP biocomposites that were produced in this work are described in Table 1. Their production involved two stages. In the first stage, the components were pre-mixed in a single-screw extruder (l/d 25/1 and a compression ratio of 3:1; Beutelspacher, Mexico City, Mexico). The mixing speed was 40 rpm, and the temperature profile from the feed zone to the die zone was 130, 140, 145, and 150°C. Throughout this step, CMP was incorporated into the PLA matrix to produce biocomposite filaments that were then pelletized. In the second stage, the formulations were processed by extrusion in a flat die to produce a laminated biocomposite that was 12 cm wide. The mixing speed was 65 rpm, and the temperature profile from the feed zone to the die zone was 150, 160, 175, and 190°C.

2.5. Characterization of PLA-CMP biocomposites

The color parameters of the biocomposites were measured with a chroma meter (Konica Minolta model CR-400) at five random points on the laminate on a white background. Based the parameters L^*, a^*, and b^*, hue angle (°Hue*), and chromaticity (C^*) were calculated using Equation 1 and Equation 2, respectively.

$$^{\circ}Hue^{*} = \arctan\left(\frac{b^{*}}{a^{*}}\right) \quad (1)$$

$$C^{*} = \left(a^{*2} + b^{*2}\right)^{1/2} \quad (2)$$

2.5.1. Apparent density

ASTM D1895-17 was used to establish the density of the biocomposites. The samples consisted of 1 × 4 cm rectangles, and their thickness was measured to calculate the volume. Subsequently, the samples were weighed on an analytical balance (Ohaus model PX2224, Parsippany, NJ, USA). Density was calculated with Equation 3 was used as follows:

$$Density = \frac{Weight\ of\ the\ sample\left(g\right)}{Volume\ of\ the\ sample\left(cm^{3}\right)} \quad (3)$$

2.5.2. Differential scanning calorimetry (DSC)

A calorimeter (Perkin Elmer model Pyris-Diamond, Boston, MA, USA) was used to determine the thermal parameters of glass transition temperature (*Tg*), crystallization temperature (*Tc*), melting temperature (*Tm*), enthalpy of

Table 1. Polylactic acid (PLA) – coconut mesocarp particle (CMP) biocomposites.

Código	PLA (wt%)	CMP (wt%)
CMP0	100	0
CMP2	98	2
CMP5	95	5
CMP8	92	8

crystallization (ΔHc), enthalpy of fusion (ΔHm), and the percentage of crystallinity. The measurement was conducted in the second heating (heat-cool-heat), in a temperature range from 0°C to 200°C, with a heating and cooling rate of 10°C/min and 50°C/min, respectively.

2.5.3. FTIR spectroscopy

FTIR spectroscopy was used to analyze the PLA–CMP biocomposites as described in section 2.2.

2.5.4. Mechanical properties

Tensile tests were performed using an universal machine (United model SSTM-5KN, Fullerton, CA, USA). The mechanical test was carried out at a crosshead speed of 5 mm/min up to sample failure. The parameters tensile strength, percentage of elongation at break, and tensile modulus were determined from the stress-strain curves. At least six rectangular specimens (1 × 6 cm) were tested at room temperature (25°C and 60% relative humidity).

2.5.5. Statistical analysis

A completely randomized design was employed, with the response variables determined by the amount of CMP (0, 2, 5, and 8 wt%) in the biocomposites. CMP0, which contained just PLA, was used as a control sample. The mean ± standard deviation of the replicates are reported for each analyzed parameter. The STATGRAPHICS PLUS 5.1 statistical program was used to perform analysis of variance (ANOVA). A p-value ($p < 0.05$) indicates statistically significant difference.

3. Results and Discussions

3.1. Characterization of CMP

Table 2 shows the proximate analysis of CMP on a dry basis (d.b.). The moisture and ash content were 7.67% and 4.59%, respectively. Compared with coconut, the natural fibers of abaca, jute, and sisal have higher moisture percentages of 15, 12.6, and 11%, respectively[7], and lower ash content of 3%, 1%, and 0.8%, respectively[8]. With respect to the ash content, CMP has more minerals than jute, sisal, hemp, cabuya, and banana stalk fibers. However, this content may vary over time; if the fiber is exposed to the environment, minerals are lost through leaching. Finally, the ether extract and protein contents of CMP are low compared with other plant products. This indicates that coconut fiber is not a source of protein and energy.

3.1.1. FTIR spectroscopy

The FTIR spectrum of CMP (Figure 1) presents the characteristic bands of cellulose and lignin structures. There is a broad absorption band at 3315 cm^{-1}, which represents the vibration of the O-H (hydroxyl) bonds; this signal is assigned to polysaccharides such as lignin, cellulose, and hemicellulose[9]. A band at 2907 cm^{-1} represents the stretching of the aliphatic group of C-H_2. The bands at 1615 cm^{-1} and 1597 cm^{-1} correspond to the vibrations of the ester (COO-) and alkene (C-C) bonds of the lignin molecule (aromatic ring), respectively. The band at 1239 cm^{-1} corresponds to the C-O groups of hemicellulose present in coconut fiber[10].

Table 2. Proximate composition of *Cocos nucifera* L. (Alto Pacifico 2 variety) mesocarp particles.

Parameters	Value (wt% dry basis)
Moisture	7.67±0.3
Ash	4.59±0.1
Ether extract	0.66±0.01
Protein	3.10±0.2

Data are presented as the mean ± standard deviation.

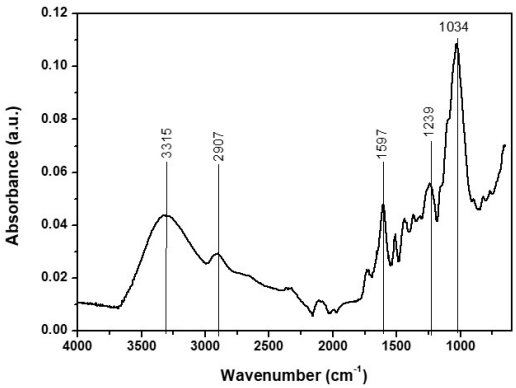

Figure 1. Fourier-transform infrared spectrum of coconut mesocarp particles.

An intense band at 1034 cm^{-1} is attributed to stretching vibrations in C-O and C-C groups present in the glycoside ring of cellulose[11]. Overall, the FTIR spectrum of CMP indicates the substantial presence of cellulose and lignin, as well as a relatively low hemicellulose content.

3.1.2. Total phenolic content

Based on the Folin-Ciocalteu method, the total phenolic content of CMP was 50.30 ± 1.6 mg gallic acid/g. This result is within the range of 25 to 78 mg gallic acid/g reported for copra, which is used for the extraction of virgin coconut oil[12]. Because the total phenolic content of CMP of the Alto Pacífico 2 variety had not been previously reported, it was compared with other agro-industrial residues. Walnut shells (58.17 ± 2.64 mg gallic acid/g) and coffee shells (52.57-97.44 mg gallic acid/g) have a slightly higher total phenolic content than of PMC. In contrast, grape pomace (10.60 ± 0.40 mg/g) and orange peel (33.24 ± 4.10 mg gallic acid/g) present a lower total phenolic content than CMP. Phenols in CMP can confer antioxidant properties. Moreover, the complex polyphenolic structure and numerous functional groups of lignin mean it could be mixed with other biopolymers to produce active films. These films contain biopolymers with bioactive compounds, allowing the controlled release of these compounds. This controlled release can extend the shelf life of food and protect it against oxidative rancidity, degradation, and discoloration.

3.1.3. Morphological characterization and elemental composition

CMP is lignocellulosic material composed of cellulose microfibrils bound together by lignin. CMP, produced from CMF, were submitted to morphological analysis.

Figure 2 shows the scanning electron micrographs of the Tyler No. 100 mesh particles at 100× (Figure 2a) and 200× (Figure 2b) magnification. In Figure 2a, there are small and large particles indicating a heterogeneous particle size distribution. Figure 2b presents a close-up of one of the larger particles showing the unit cell structure of the exfoliated, which are in the form of overlapping sheets and plates. The exfoliated structures correspond to non-fibrous particles; it is assumed that they are coated by layers that are rich in hemicellulose and lignin. Moreover, these structures provide rigidity to the cellulose–hemicellulose–lignin network, which showing a rough surface[13].

The elemental composition of the coconut particles is presented in Figure 3. This analysis was performed on the surface of the sample (inset image). The elements present in the spectrum are carbon, potassium, oxygen, sodium, silicon, and chlorine; sodium and silicon are present in trace amounts. The presence of sodium and potassium is mainly attributed to the salinity of the CMF powder[14]. The table in Figure 3 shows that the major element is carbon, followed by oxygen; together, these elements represent 96.75% of the weight. The atomic O/C ratio of coconut particles is 0.57, which is lower than pineapple husk (0.70) and coffee husk (0.71). According to Ugwu and Enweremadu[15], the higher the atomic O/C ratio, the lower the calorific value; therefore, the oxygen in the residue does not contribute to the calorific value in the agro-industrial residue.

3.2. Characterization of the PLA-CMP biocomposites

3.2.1. Color and density

In the PLA–CMP biocomposites, L^* and °Hue* decreased gradually as the CMP content increased. The brightness of CMP0 (which only contained PLA) was significantly different ($p < 0.05$) from CMP2, CMP5, and CMP8. This difference is because CMP do not reflect light and the PLA–CMP biocomposites behave as an opaque material.

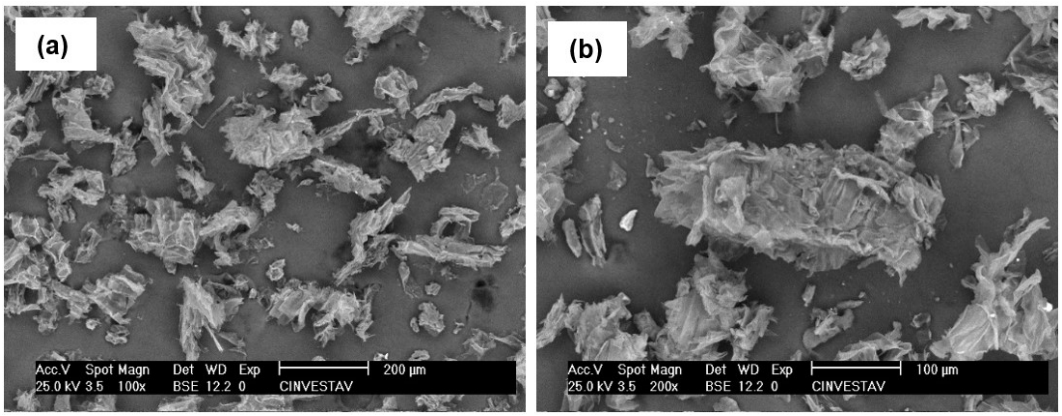

Figure 2. Scanning electron micrographs of coconut mesocarp particles at 100× (a) and 200× (b) magnification.

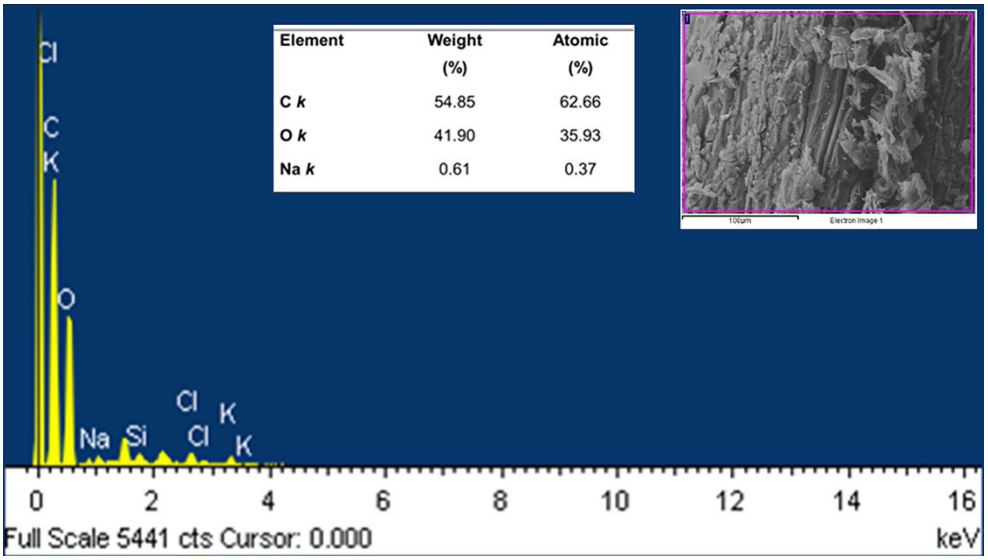

Figure 3. Elemental composition of coconut mesocarp particles.

CMP0 (only PLA) presented a C^* value close to 0, which indicates that there is a tendency for it to be white. The C^* value increased in the PLA–CMP biocomposites as the CMP content increased; it was significantly different ($p < 0.05$) in CMP2, CMP5, and CMP8 compared with CMP0. C^* was not significantly different ($p > 0.05$) between CMP5 and CMP8; both films had a brownish chroma. CMP0 had a white shade and a significantly different °Hue* ($p < 0.05$) compared with CMP2, CMP5, and CMP8, which presented a yellowish shade. There was a significant difference ($p < 0.05$) in °Hue*. The °Hue* and C^* parameters confirms that the brown (red-yellow) shade of CMP8. Figure 4 shows the images of the formulated biocomposites.

Table 3 also presents the density of each formulation. Given that the density of the PLA matrix is 0.95 g/cm^3 and the density of the CMP is 0.145 g/cm^3, the addition of CMP decreased the density of the biocomposites. There was an increase in density from CMP2 to CMP5 because CMP occupy a larger volume but are distributed throughout the PLA matrix, occupying all the space. The subsequent decrease in density in CMP8 is due to poor displacement of CMP, leading to empty spaces in which the air is trapped inside the material.

3.2.2. Thermal characterization

Table 4 presents the thermal analysis of the formulations determined with DSC. *Tg*, *Tc*, *Tm*, Δ*Hc*, and Δ*Hm* were obtained from the thermograms of the second heating of the biocomposites. *Tg* of the PLA matrix (CMP0) was 58.45°C; it is similar for CMP2 and CMP5, but decreased slightly, to 57.33°C, for CMP8. The *Tg* result indicate that there is compatibility at the PLA matrix–CMP interface[16].

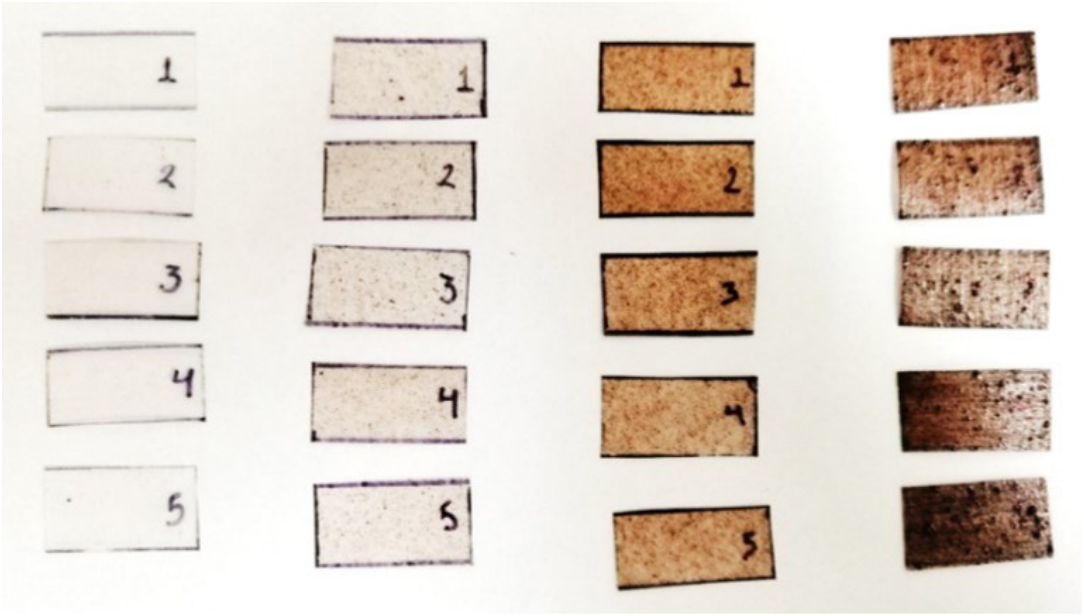

Figure 4. Images of the polylactic acid (PLA)–coconut mesocarp particle (CMP) biocomposites. From left to right: CMP0 (PLA only), CMP2, CMP5, and CMP8.

Table 3. Color parameters (L^*, C^*, and °Hue*) and the density of polylactic acid (PLA) and coconut mesocarp particle (CMP) biocomposites.

Formulation	L^*	C^*	°Hue*	Density (g/cm^3)
CMP0	92.27±1.01 ^{d}	1.48±0.31 ^{a}	138.74±2.01 ^{c}	0.95±0.06 ^{c}
CMP2	78.27±2.13 ^{c}	6.74±0.25 ^{b}	33.11±1.75 ^{b}	0.40±0.07 ^{a}
CMP5	63.63±2.51 ^{b}	17.59±0.43 ^{c}	31.53±1.48 ^{b}	0.60±0.04 ^{b}
CMP8	11.81±1.83 ^{a}	17.29±0.47 ^{c}	12.61±1.65 ^{a}	0.41±0.05 ^{a}

The data are presented as the mean ± standard deviation. Different letters in the same column indicate a significant difference ($p < 0.05$).

Table 4. Thermal parameters of polylactic acid (PLA)–coconut mesocarp particles (CMP) biocomposites.

Formulation	*Tg* (°C)	*Tc* (°C)	*Tm* (°C)	Δ*Hc* (J/g)	Δ*Hm* (J/g)
CMP0	58.45	123.02	148.32	23.02	21.03
CMP2	58.70	120.01	147.26	26.82	27.75
CMP5	58.33	119.60	147.01	21.54	22.73
CMP8	57.33	119.03	147.28	25.52	28.07

A decrease in *Tg* in biocomposites has been reported in PLA systems and other agro-industrial wastes and indicates possible interactions between the components[17].

Tc in the PLA matrix (CMP0) was 123°C and decreased gradually as the amount of CMP in the PLA–CMP biocomposite increased. This indicates that there is a decrease in the temperature at which cold crystallization of PLA occurs because the particles act as nucleating agents that induce the formation of crystalline phases around them. *Tm* behave similarly to *Tg* because the fraction of PLA that melts has a lower fraction of crystalline phase in the biocomposite. Δ*Hc* and Δ*Hm* show an increase and decrease, respectively, as the amount of CMP in the PLA–CMP biocomposites increased. This apparent anomalous behavior is due to the distribution of crystalline phases in the biocomposite; CMP restrict the mobility of the chains. The biocomposites with a lower CMP content have greater crystallinity because there are more PLA chain–CMP interactions. In CMP8, CMP tend to agglomerate, generating crystalline phases in the matrix, sot there is an increase in Δ*Hc* and Δ*Hm*. Hassain et al.[18] reported similar behavior.

3.2.3. Structural characterization

The FTIR spectra of the biocomposites are shown in Figure 5. The biocomposites spectra show the same band pattern because the particles are encapsulated within the PLA matrix. Overall, the addition of CMP does not have a significant effect on CMP (PLA only) spectrum. A band at 2916 cm^{-1} is attributed to asymmetric methylene stretching vibrations. The band at 2850 cm^{-1} is attributed to symmetric methylene stretching vibrations. These bands are present in the biocomposites, although they are less intense.

The sharp and prominent band at 1753 cm^{-1} corresponds to the stretching of the carbonyl groups (C=O) of the PLA ester group. The bands at 1450 and 1356 cm^{-1} correspond to the asymmetric C-H deformation of the methyl group (CH_3). The stretching modes of the C-O signal of the PLA ester group appear at 1225 cm^{-1}, and the asymmetric mode of the C-O-C signal appears at 1090 cm^{-1}. Other notable bands are at 956 and 921 cm^{-1}, due to the secondary signals of the CH_3 group and corresponding to the vibrations in the main chain of the CH_3 group. There are bands at 871 and 756 cm^{-1} that can be attributed to the amorphous and crystalline phases of PLA, respectively[18].

3.2.4. Mechanical properties

Figure 6 shows the tensile strength, elongation at break, and tensile modulus obtained from the mechanical tests of the biocomposites. The tensile strength of the biocomposites decreased significantly ($p < 0.05$) in CMP2, CMP5, and CMP8 compared with CMP0. There was no significant difference ($p > 0.05$) between CMP2 and CMP5, and CMP8 presented the lowest tensile strength. This is explained by the fact that while CMP are dispersed throughout the matrix at lower concentrations, they also show the development of agglomerations in the biocomposites and the creation of areas of stress concentration as the CMP content increases. Furthermore, the inadequate stress transfer caused by the weak interfacial adhesion between the PLA matrix and the dispersed phase of CMP inhibits CMP from acting as a reinforcing agent. Islam et al.[19] observed a decrease in tensile strength in polypropylene composites and coconut particles without surface modification; they attributed it to the weak particle–matrix interactions.

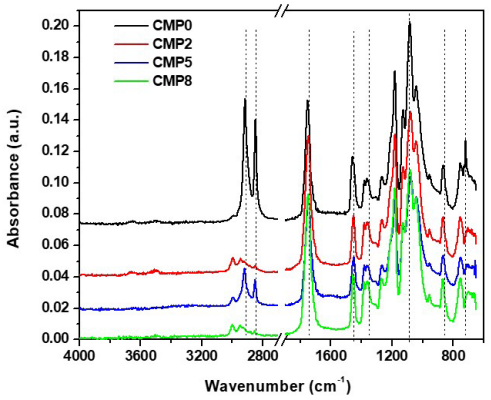

Figure 5. Fourier-transform infrared spectra of the polylactic acid (PLA)–coconut mesocarp particle (CMP) biocomposites.

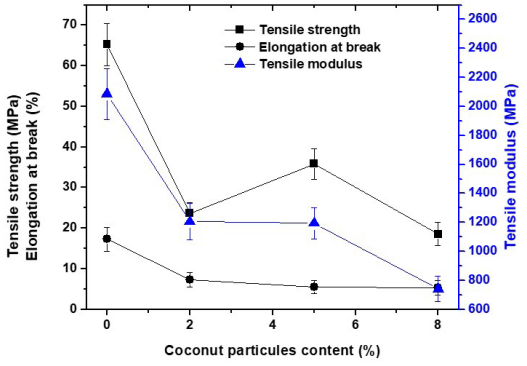

Figure 6. Mechanical parameters of the polylactic acid (PLA)–coconut mesocarp particle (CMP) biocomposites.

The elongation at break showed a 55% reduction in CMP2, but it was not reduced in CMP5 and CMP8. This could be attributed to the irregular shape of the particles and the discontinuity in the matrix caused by CMP, which weakens the biocomposite and makes it brittle. The elastic modulus (Figure 6) decreased significantly ($p < 0.05$) when CMP was incorporated into the PLA matrix. There was not a significant difference between CMP2 and CMP5 ($p < 0.05$) in this parameter. This can be attributed to the lack of adequate adhesion between CMP and the PLA matrix, resulting in a weak particle–matrix interactions[20]. In addition, an increase in the CMP content weakens the fiber–matrix interactions as well as cohesion, leading to a decreasing trend in tensile strength as well as a decrease in the amount of polymer matrix for material elongation[21]. The stiffness of a material is critical to determine its application, so the elastic modulus is the primary parameter analyzed in the selection of a material. The dispersion and adhesion of CMP in the PLA matrix are critical factors that determine the mechanical properties of biocomposites.

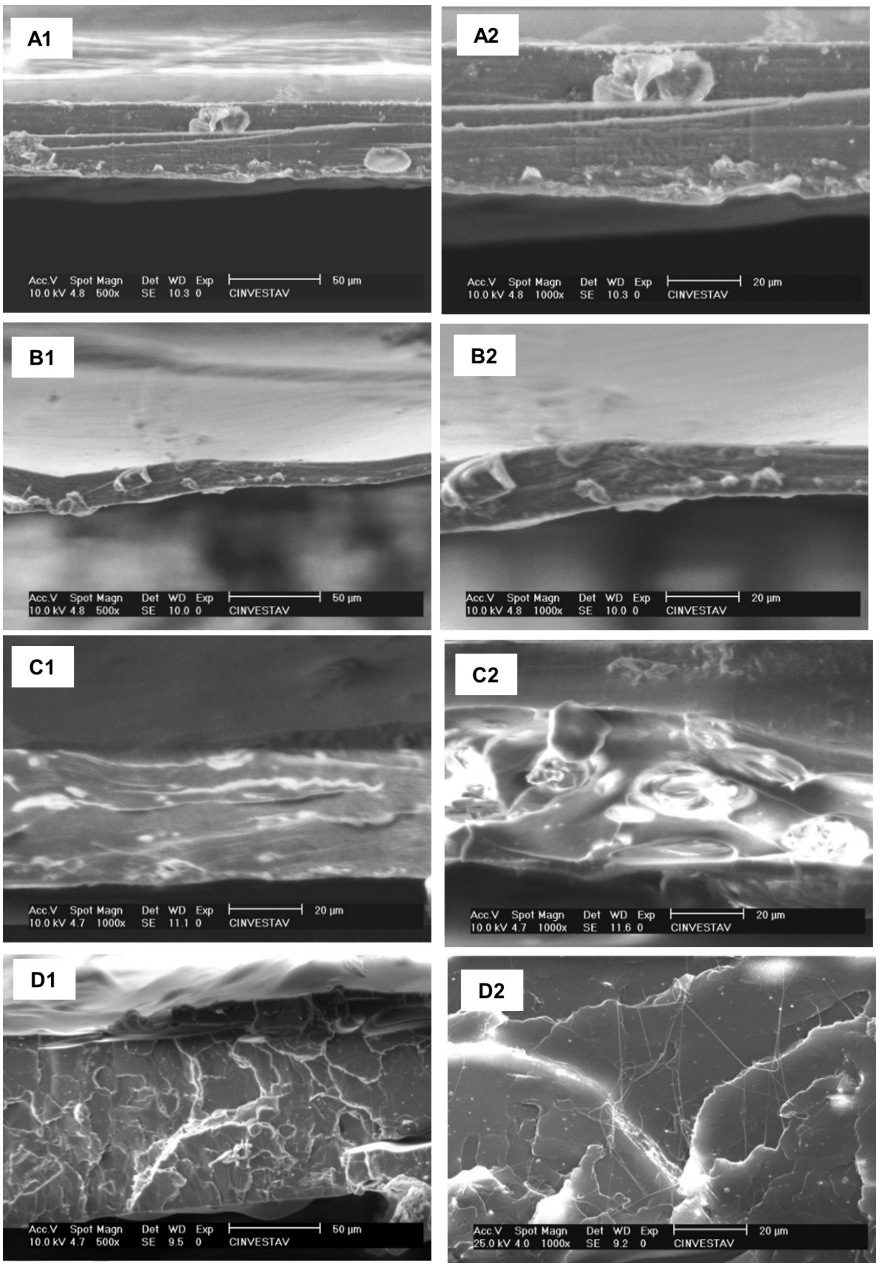

Figure 7. Scanning electron micrograph of polylactic acid (PLA)—coconut mesocarp particle (CMP) biocomposites: CMP0 (A), CMP2 (B), CMP5 (C), and PMC8 (D) at 500× (1) y 1000× (2) magnification.

3.2.5. Morphological characterization of the biocomposites

Scanning electron microscopy analysis of the fracture surfaces was performed on the biocomposites subjected to tension. Figure 7(A1) and 7(A2) show the surface roughness of CM0 (PLA only), which is typical of a plastic fracture of a thermoplastic polymer under a low stretching rate. This characteristic is homogeneous along the fracture surface of the sample. Madera-Santana et al.[17] reported a similar result with PLA—algal residue biocomposites. Figure 7(B1) and 7(B2) correspond to CMP2; in the fracture surface area, there is a rough surface accompanied by very few CMP. Figure 7(C1) and 7(C2), correspond to CMP5. CMP are distributed in the matrix; in addition, there are some spaces between CMP and the PLA matrix, which indicate deficient particle—matrix interfacial adhesion. Figure 7(D1) and 7(D2) show CMP8 micrographs. The matrix shifts from plastic to a brittle fracture; in addition, there are some pores on the surface and filaments of the PLA matrix. These empty spaces (pores) are generated by the detachment of CMP from the PLA matrix. These weak zones are closely correlated with the strength of the matrix, which gradually decrease the strength of the biocomposite[21]. Importantly, the detachment of matrix particles in biocomposites indicates brittle fracture of the

material. However, the roughness of CMP may favor their mechanical adhesion to the matrix.

4. Conclusions

Proximate analysis of CMP revealed that they have limited nutritional value, so their application for the manufacture of biocomposites is an alternative. Hence, PLA—CMP biocomposites were produced via extrusion.

The brownish color in the biocomposites was caused by CMP inclusion. The biocomposites showed a gradual decrease in tensile strength as the CMP content increased. The elongation at break of the biocomposites decreased significantly compared with the PLA matrix, although they did not differ significantly from each other. CMP5 presented the highest elastic modulus among the biocomposites. The crystallinity of the biocomposites decreased as the amount of CMP increased, which indicates that the particles act as nucleating agents, restricting the mobility of the PLA chains. The FTIR spectra of the biocomposites present similar bands to the PLA matrix spectrum because CMP are embedded in the polymer. Some PLA functional group signals exhibit slight shifts in location and intensity, which may be explained by interactions between the PLA matrix and CMP. According to the results obtained in this work, CMP and PLA can form a biocomposite with suitable physicochemical properties for use as rigid packaging for food or other biodegradable products.

5. Author's Contribution

• **Conceptualization –** Luz del Carmen Montoya-Ballesteros; Tomás Jesús Madera-Santana.

• **Data curation –** Yulinali Valente-Morales; Yesica Yudith Martínez Núñez; Judith Fortiz Hernández; Luis Enrique Robles-Ozuna.

• **Formal analysis –** Luz del Carmen Montoya-Ballesteros; Tomás Jesús Madera-Santana.

• **Funding acquisition –** Luz del Carmen Montoya-Ballesteros.

• **Investigation –** Yulinali Valente-Morales; Yesica Yudith Martínez Núñez; Judith Fortiz Hernández; Luis Enrique Robles-Ozuna.

• **Methodology –** NA.

• **Project administration –** Tomás Jesús Madera-Santana.

• **Resources –** Luz del Carmen Montoya-Ballesteros; Tomás Jesús Madera-Santana; José Carmelo Encinas-Encinas.

• **Software –** NA.

• **Supervision –** Luz del Carmen Montoya-Ballesteros; Tomás Jesús Madera-Santana.

• **Validation –** NA.

• **Visualization –** Luz del Carmen Montoya-Ballesteros; Tomás Jesús Madera-Santana.

• **Writing – original draft –** Yulinali Valente Morales; Tomás Jesús Madera-Santana

• **Writing – review & editing –** Luz del Carmen Montoya-Ballesteros; José Carmelo Encinas-Encinas.

6. Acknowledgements

Part of this research was conducted at the facilities of Laboratorio Nacional CONACYT LANNBIO-Cinvestav Unidad Mérida (PROY. No. 321119).

7. References

1. Koul, B., Yakoob, M., & Shah, M. P. (2022). Agricultural waste management strategies for environmental sustainability. *Environmental Research*, *206*, 112285. http://doi.org/10.1016/j.envres.2021.112285. PMid:34710442.
2. Esparza, I., Jiménez-Moreno, N., Bimbela, F., Ancín-Azpilicueta, C., & Gandía, L. M. (2020). Fruit and vegetable waste management: conventional and emerging approaches. *Journal of Environmental Management*, *265*, 110510. http://doi.org/10.1016/j.jenvman.2020.110510. PMid:32275240.
3. Torres-Giner, S., Hilliou, L., Meléndez-Rodríguez, B., Figueroa-López, K. J., Madalena, D., Cabedo, L., Covas, J. A., Vicente, A. A., & Lagaron, J. M. (2018). Melt processability, characterization, and antibacterial activity of compression-molded green composite sheets made of poly(3-hydroxybutyrate-co-3-hydroxyvalerate) reinforced with coconut fibers impregnated with oregano essential oil. *Food Packaging and Shelf Life*, *17*, 39-49. http://doi.org/10.1016/j.fpsl.2018.05.002.
4. Burrola-Núñez, H., Herrera-Franco, P. J., Rodríguez-Félix, D. E., Soto-Valdez, H., & Madera-Santana, T. J. (2019). Surface modification and performance of jute fibers as reinforcement on polymer matrix: an overview. *Journal of Natural Fibers*, *16*(7), 944-960. http://doi.org/10.1080/15440478.2018.1441093.
5. Rosa, M. F., Chiou, B.-S., Medeiros, E. S., Wood, D. F., Williams, T. G., Mattoso, L. H. C., Orts, W. J., & Iman, S. H. (2009). Effect of fiber treatments on tensile and thermal properties of starch/ethylene vinyl alcohol copolymers/coir biocomposites. *Bioresource Technology*, *100*(21), 5196-5202. http://doi.org/10.1016/j.biortech.2009.03.085. PMid:19560341.
6. Singleton, V. L., Orthofer, R., & Lamuela-Raventós, R. M. (1999). Analysis of total phenols and other oxidation substrates and antioxidants by means of Folin-Ciocalteu Reagent. *Methods in Enzymology*, *299*, 152-178. http://doi.org/10.1016/S0076-6879(99)99017-1.
7. Ramamoorthy, S. K., Skrifvars, M., & Persson, A. (2015). A review of natural fibers used in biocomposites: Plant, animal and regenerated cellulose fibers. *Polymer Reviews (Philadelphia, Pa.)*, *55*(1), 107-162. http://doi.org/10.1080/15583724.2014.971124.
8. Li, X., Tabil, L. G., & Panigrahi, S. (2007). Chemical treatments of natural fiber for use in natural fiber-reinforced composites: a review. *Journal of Polymers and the Environment*, *15*(1), 25-33. http://doi.org/10.1007/s10924-006-0042-3.
9. Vidal, N. E. H., Bautista, V. L., Morales, V. M., Ordoñez, W. M., & Osorio, E. S. C. (2018). Chemical characterization of coco fiber (Cocos nucifera L.) from Mexico using Infrared Spectroscopy (FTIR). *Revista Ingeniería y Región*, *20*, 67-71. Retrieved in 2024, August 20, from https://dialnet.unirioja.es/servlet/articulo?codigo=7059315
10. Célino, A., Goncalves, O., Jacquemin, F., & Fréour, S. (2014). Qualitative and quantitative assessment of waters sorption in natural fibres using ATR FTIR spectroscopy. *Carbohydrate Polymers*, *101*, 163-170. http://doi.org/10.1016/j.carbpol.2013.09.023. PMid:24299761.
11. Abraham, E., Deepa, B., Pothen, L. A., Cintil, J., Thomas, S., John, M. J., Anandjiwala, R., & Narine, S. S. (2013). Environmental friendly method for the extraction of coir fibre and isolation of nanofibre. *Carbohydrate Polymers*, *92*(2),

1477-1483. http://doi.org/10.1016/j.carbpol.2012.10.056. PMid:23399179.

12. Marina, A. M., Che Man, Y. B., Nazimah, S. A., & Amin, I. (2009). Antioxidant capacity and phenolic acids of virgin coconut oil. *International Journal of Food Sciences and Nutrition*, *60*(2, Suppl 2), 114-123. http://doi.org/10.1080/09637480802549127. PMid:19115123.
13. Olorunnisola, A. O. (2009). Effects of husk particle and calcium chloride on strength and sorption properties of coconut husk-cement composites. *Industrial Crops and Products*, *29*(2-3), 495-501. http://doi.org/10.1016/j.indcrop.2008.09.009.
14. Abad, M., Noguera, P., Puchades, R., Maquieira, A., & Noguera, V. (2002). Physico-chemical and chemical properties of some coconut coir dusts for use as a peat substitute for containerised ornamental plants. *Bioresource Technology*, *82*(3), 241-245. http://doi.org/10.1016/S0960-8524(01)00189-4. PMid:11991072.
15. Ugwu, S. N., & Enweremadu, C. C. (2020). Ranking of energy potentials of agro-industrial wastes: bioconversion and thermo-conversion approach. *Energy Reports*, *6*, 2794-2802. http://doi.org/10.1016/j.egyr.2020.10.008.
16. Tognana, S., Salgueiro, W., & Somoza, A. (2007). Influencia del proceso de curado y del contenido de carga sobre la Tg y el volumen libre en compuestos particulados de matriz epoxi. *Revista Matéria (Rio de Janeiro)*, *12*(3), 510-517. http://doi.org/10.1590/S1517-70762007000300012.
17. Madera-Santana, T. J., Freile-Pelegrín, Y., Encinas, J. C., Ríos-Soberanis, C. R., & Quintana-Owen, P. (2015). Biocomposites based on poly(lactic acid) and seaweed wastes from agar extraction: evaluation of physicochemical properties. *Journal of Applied Polymer Science*, *132*(31), 42320. http://doi.org/10.1002/app.42320.
18. Hassain, K. M. Z., Parsons, A. J., Rudd, C. D., Ahmed, I., & Thielemans, W. (2014). Mechanical, crystallisation and moisture absorption properties of melt drawn poly(lactic) acid fibres. *European Polymer Journal*, *53*, 270-281. http://doi.org/10.1016/j.eurpolymj.2014.02.001.
19. Islam, N., Rahman, R., Haque, M., & Huque, M. (2010). Physico-mechanical properties of chemically treated coir reinforced polypropylene composites. *Composites Part A: Applied Science and Manufacturing*, *41*(2), 192-198. http://doi.org/10.1016/j.compositesa.2009.10.006.
20. Marinho, J. F., Braga, N. F., Krohn, A., Myata, F. S., Silveira, L. H., Cabral, A., No., & Fechine, G. J. M. (2015). Melt processing of polymers biocomposites. *Polímeros: Ciência e Tecnologia*, *25*(2), 133-136. http://doi.org/10.1590/0104-1428.1847.
21. Nam, T. H., Ogihara, S., Tung, N. H., & Kobayashi, S. (2011). Effect of alkali treatment on interfacial and mechanical properties of coir fiber reinforced poly(butylene succinate) biodegradable composites. *Composites Part B: Engineering*, *42*(6), 1648-1656. http://doi.org/10.1016/j.compositesb.2011.04.001.

Received: Mar. 20, 2024
Revised: May 02, 2024
Accepted: May 04, 2024